Composites Part C: Open Access 18 (2025) 100667

Contents lists available at ScienceDirect

Composites Part C: Open Access

journal homepage: www.elsevier.com/locate/composites-part-c-open-access

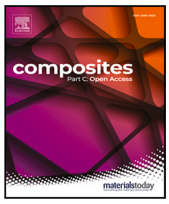

Coelacanth-scale inspired thin-ply composites for load-bearing applications

Marcel Neubacher [a,*], Farida Touni [a], Kohei Yamada [b], Masaaki Nishikawa [c], Bodo Fiedler [a]

[a] Institute of Polymers and Composites, Hamburg University of Technology, Denickestraße 15, Hamburg, 21073, Hamburg, Germany
[b] Industrial Technology Center of Fukui Prefecture, Kawaiwashizuka 61-10, Kawaiwashizuka, 910-0102, Fukui, Japan
[c] Department of Mechanical Engineering and Science, Kyoto University, Kyotodaigaku-katsura C3, Nishikyo-ku, 615-8540, Kyoto, Japan

ARTICLE INFO

Keywords:
Bio-inspired
Bouligand
CFRP
CLT
Load introduction

ABSTRACT

Thin-ply composites are known for their superior in-situ strength and manufacturing quality, offering higher unnotched tensile and compressive strengths compared to conventional laminates. However, their damage suppression capability leads to increased notch sensitivity, where the delamination and matrix cracking mechanisms are suppressed. As a result, thin-ply laminates are limited in their use in critical load-bearing applications. To address this, bio-inspired Bouligand structures, defined by their helical fibre arrangements, have shown promise in reducing notch sensitivity through helicoidal matrix cracking and stress redistribution. This study explores the mechanical performance of partial Bouligand layups derived from biological fibre architectures observed on coelacanth fish scales, where fibrils reorient under load. An analytical stiffness-based optimization was performed to match the mechanical properties of the conventional [0°, ±45°, 90°] (50 %, 40 %, 10 % load introduction layup used in bolted and riveted aircraft structures, while integrating the partial Bouligand structure. The weights of the two-layer fibres (30 gsm and 60 gsm) were investigated, resulting in different pitch and stack angles. Tensile and bearing tests were conducted to evaluate the influence of the partial Bouligand structure on bearing sensitivity. The results indicate that bio-inspired fibre orientation can improve load redistribution and damage tolerance in thin-ply laminates, making them compatible for off-axis and notched applications.

1. Introduction

Thin-ply carbon fibre reinforced polymers (CFRPs), produced using techniques such as spread-tow processes, have emerged as a high performance alternative to conventional composites, with individual ply thicknesses starting from 20 µm [1,2]. The reduction in ply thickness enables greater design flexibility by increasing the number of plies within a laminate and allowing for more precise tailoring of fibre orientations based on load paths.

Thin-ply laminates also demonstrate superior in-situ strength, suppressing mechanisms such as transverse microcracking and free-edge delamination [1]. This results in a transition in failure behaviour from delamination-dominated modes in thick plies to more brittle, fibre-dominated failure in thin plies, leading to higher ultimate tensile and compressive strengths in unnotched quasi-isotropic and unidirectional laminates [3–5]. In addition to an optimized mechanical performance, thin-ply laminates benefit from improved manufacturing quality, including lower void content, better fibre alignment, and reduced resin-rich zones [3].

However, despite these advantages, thin-ply laminates often exhibit heightened notch sensitivity, particularly in tension, which can lead to premature and brittle failure when stress concentrations are introduced, such as holes or impact damage [1]. Thin-ply laminates tend to exhibit a lower ultimate open hole tensile strength (OHT), up to 30 % less than thick plies, as they suppress damage mechanisms such as delamination and interfibre cracking, which conventionally help redistribute stress around the notches [5,6]. This results in a pronounced notch sensitivity, where the strength and stiffness of the composites drop significantly near the stress concentrators, reducing the effective load that the structure can carry safely. To address this challenge, structural modifications that reintroduce controlled damage mechanisms have been proposed. Among the most promising approaches are bio-inspired fibre architectures, such as Bouligand (helicoidal) layups, which gradually rotate fibre orientations between adjacent plies [7–10]. Bouligand composites demonstrate superior performance and damage tolerance under OHT loading compared to quasi-isotropic (QI) and traditional cross-ply laminates. As shown in [8], thin-ply Bouligand structures with

* Corresponding author.
E-mail address: marcel.neubacher@tuhh.de (M. Neubacher).

https://doi.org/10.1016/j.jcomc.2025.100667
Received 21 August 2025; Received in revised form 29 September 2025; Accepted 16 October 2025
Available online 18 October 2025

extremely low pitch angles mimic biological fibre arrangements and exhibit fundamentally different failure behaviour. Instead of abrupt delamination, they develop diffused, helicoidal matrix cracking that spreads stress and dissipates energy, resulting in low notch sensitivity despite the reduced 0° fibre content. Further research [11] showed that, unlike cross-ply laminates which suffer from brittle or pull-out failure depending on fibre angle, Bouligand layups maintain more stable spiral fracture patterns across varying off-axis angles. This leads to better balanced strength and improved structural reliability in notched and multiaxial loading scenarios, making Bouligand designs well suited for advanced load-bearing applications.

Load-bearing stresses in composite materials occur in areas of bolted and riveted joints. These joints are characterized by their straightforward installation and removability, making them cost-effective solutions that are widely used, particularly in the aerospace industry [12–16]. The studies by [17,18] investigate quasi-isotropic thick- and thin-ply laminates using single shear bearing tests. The published results show that thin-ply laminates exhibit a delayed onset of damage of 47.00 % [17], while [18] observed a previous first failure. Despite these differences, the determined ultimate bearing strengths of thin-ply laminates with approximately 40 gsm in both studies are comparable, being 14.47 % [17] and 15.30 % [18] higher than those of thick-ply reference laminates with approximately 160 gsm. In this context, [5] reported an increase in ultimate bearing strength of 20.00 % for intermediate-ply laminates with 100 gsm and 23.00 % for thin-ply laminates with 30 gsm compared to thick-ply laminates with 300 gsm, which exhibited an ultimate bearing strength of 476 MPa. The described behaviour can be explained by the fact that thin plies are capable of delaying or even suppressing subcritical and progressive damage mechanisms such as delamination, matrix cracks, fibre buckling, and shear cracks [3–5]. Furthermore, thinner plies lead to reduced shear stresses within the laminate due to the higher number of ply interfaces [3], which in turn results in increased loadings onset of delamination [3,5]. The result is an improved load-bearing capacity of laminates with thinner plies [3,4].

Previous studies have predominantly focused on structures subjected to a constant load orientation. However, in rotationally movable components, such as aircraft air brakes, the direction of the load can vary during operation due to the presence of a hinge. Under these conditions, typical quasi-isotropic or load-introductory laminate structures experience off-axis loading. Research [11] has shown that the mechanical strengths of cross-ply laminates significantly degrade under off-axis stress. In contrast, Bouligand structures do not exhibit this effect, as their fibres are distributed rotationally with much smaller angular increments, resulting in nearly isotropic material behaviour and thus enhanced capacity to accommodate off-axis loads [11].

In addition to fully developed Bouligand structures, nature has also produced structures during evolution that are specifically designed for certain load cases. A remarkable example of this can be found in coelacanth fish scales. In an unloaded state, the tissue of the fish scale shows a so-called double twisted Bouligand structure [19–21]. The double twisted Bouligand structure of the coelacanth fish has been previously investigated in three-point bending and charpy impact tests, as reported in [21]. As [19] was able to demonstrate using in-situ synchrotron SAXS during tensile tests, the fibrils orient themselves in the direction of the mechanical stress. The orientation of the fibrils under load application is shown in Fig. 1. The in-situ synchrotron SAXS measurements indicate that the fish scale forms an oriented Bouligand structure, hereafter called a partial Bouligand structure, under uniaxial tensile stress. This structure extends over an angular range of ±60°, with the strongest fibril alignment occurring in the range of ±40° compared to the unloaded scale. A comparison of fibril orientation under uniaxial tensile load with the stress distribution of a composite bolted join shown in Fig. 2 right shows similarity.

In this study, the partial Bouligand structure of the coelacanth-scale is replicated for engineering applications, fibre angles of ±60°

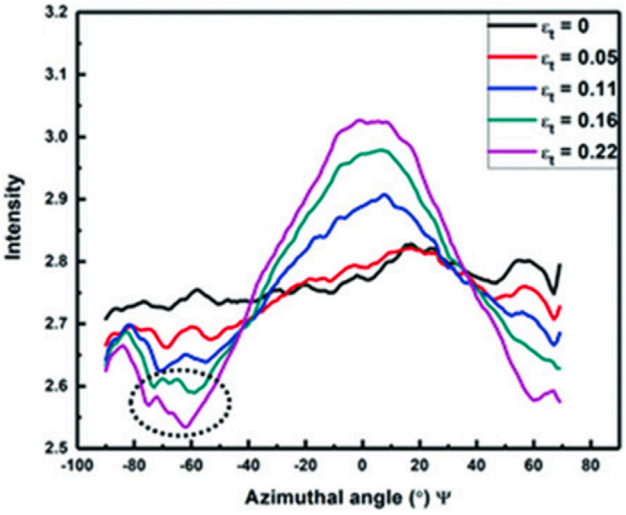

Fig. 1. Diffraction intensity over fibrill angle of Coelacanth-scale [19].

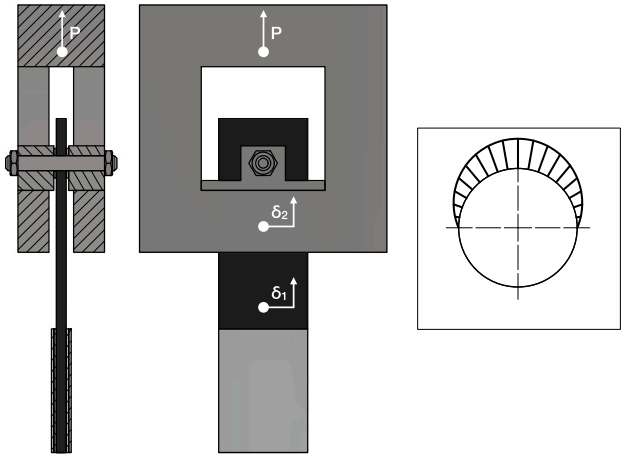

Fig. 2. Schematic setup of the bearing test and stress distribution in the laminate around the hole.

and ±40°, as observed on the fish scale, were combined with the traditional load introduction (LI), a structure commonly used in composite laminates with bolted joints and open holes. The conventional LI layup, established in the aviation industry and widely applied to promote bearing failure while suppressing other failure modes, serves as a benchmark for comparison in this study, with the following layer configurations [12,13]:

30 gsm: $[45, 0, -45, 0, 90, 0, 45, 0, -45, 0]_{6s}$

60 gsm: $[45, 0, -45, 0, 90, 0, 45, 0, -45, 0]_{3s}$

When designing composite materials, stiffness is an important design criterion in addition to strength. This includes thin plates, where buckling must be prevented and openings whose geometry must remain stable, such as aircraft door frames. This study investigates how the stiffness properties of a conventional LI layup can be modified by transforming it into a Bouligand structure. On this basis, a stiffness optimization was carried out using classical laminate theory (CLT) in order to develop a partial Bouligand structure $\sum_{k=0}^{i}(\alpha - k \cdot \theta)$, where α represents the stack angle and θ the pitch angle, with comparable stiffness properties. A schematic representation of a partial Bouligand structure is shown in Fig. 3.

Two different optimization approaches were selected. The first approach focused on optimizing the elastic properties A_{11} and A_{22}. The

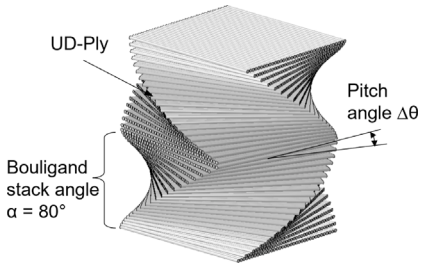

Fig. 3. Schematic representation of a partial Bouligand structure.

Table 1
Material parameters employed for stiffness optimization using CLT.

FAW in gsm	E_L in GPa	E_T in GPa	ν_{LT}	G_{LT} in GPa
30	137.14	7.86	0.33	3.85
60	132.59	8.38	0.33	3.85

corresponding objective function was defined as follows:

$$f(\alpha,\theta) = \left|\frac{A_{11\_BI}}{A_{11\_LI}}\right| + \left|\frac{A_{22\_BI}}{A_{22\_LI}}\right| \tag{1}$$

The following layup configurations were derived based on the minimization function and show a close correspondence to the ±60° oriented fibrillar structure observed in the fish scale:

30 gsm: $\left[\sum_{k=0}^{59}(64.9° - k \cdot 2.2°)\right]_s$

60 gsm: $\left[\sum_{k=0}^{29}(63.8° - k \cdot 4.4°)\right]_s$

The second optimization approach aimed to optimize the stiffness in the main load direction. For this purpose, the effective stiffness E_{11} was considered according to the relationship $E_{11} = \frac{1}{h} \cdot \left(A_{11} \cdot \frac{A_{12}^2}{A_{22}}\right)$ and the following minimization function was applied:

$$f(\alpha,\theta) = \left|E_{11\_BI} - E_{11\_LI}\right| \tag{2}$$

Based on this minimization function, the following layup configuration was obtained that aligns closely with the highly oriented fibril angle ±40° observed in the fish scale:

60 gsm: $\left[\sum_{k=0}^{28}(40.5° - k \cdot 2.9°)\right]_s$

2. Materials and methods

2.1. Materials and specimen preparation

The material used in the present study consists of unidirectional prepregs with two different fibre areal weights (30 gsm and 60 gsm). These prepregs were manufactured by North Thin Ply Technology (NTPT) and comprise Toray S700SC-12K-60E carbon fibres and NTPT ThinPreg 402 epoxy resin. Table 1 presents the material parameters used in the CLT-based stiffness optimization.

The laminate structures shown in Table 2 were produced using the hand lay-up process and then cured in an autoclave according to the manufacturer's specifications. The cured panels were cut into specimens using a water-cooled Brillant 265 circular saw from ATM Qness GmbH, equipped with a diamond cutting disc, at a constant feed rate of 1.0 mm/s. After cutting, all edges of the specimen were polished with a grit size of P1000. For bearing samples, the holes were precisely machined by helical milling utilizing a 2 mm diameter solid carbide miniature end mill (Karnasch Professional Tools GmbH) mounted on an EUROMOD®-MP CNC milling machine (Isel Germany AG, Eichenzell, Germany). In the clamping jaw region, the specimens were mechanically reinforced with a 1 mm thick layer of glass fibre reinforced polymer (GFRP) and a 1 mm thick aluminum layer. Subsequently, the tabs were adhesively bonded using two-component UHU PLUS Endfest 300 adhesive in a hot press to ensure a durable connection. Before testing, all samples were conditioned for 48 h at 40 °C under vacuum to ensure consistent material properties. All tests were carried out under standard laboratory conditions of 20 °C and 50% relative humidity.

Table 2
Overview of the investigated configurations, including layup details, fibre areal weight (faw) and nominal specimen thicknesses h.

Configuration	faw	Lay-up	h in mm
30_LI	30 gsm	$[45, 0, -45, 0, 90, 0, 45, 0, -45, 0]_{6s}$	3.60
60_LI	60 gsm	$[45, 0, -45, 0, 90, 0, 45, 0, -45, 0]_{3s}$	3.60
30_BI_1	30 gsm	$\left[\sum_{k=0}^{59}(64.9° - k \cdot 2.2°)\right]_s$	3.60
60_BI_1	60 gsm	$\left[\sum_{k=0}^{29}(63.8° - k \cdot 4.4°)\right]_s$	3.60
60_BI_2	60 gsm	$\left[\sum_{k=0}^{28}(40.5° - k \cdot 2.9°)\right]_s$	3.48

2.2. Experimental methods

To evaluate the mechanical strength and damage tolerance of the Bouligand structures compared to conventional designs, experimental tests were conducted following ASTM D3039 [22] for unnotched tension (UNT) and ASTM D5961 Procedure A (Double Shear Test) [23] for bearing performance.

UNT tests were performed using a ZwickRoell Z100 universal testing machine (maximum load 100 kN) equipped with hydraulic grips. The tensile test was carried out at a constant crosshead speed of 2 mm/min and the strain was measured using a multiXtens extensometry system.

Bearing tests were carried out using a double shear clevis fixture and a ZwickRoell Z400 machine (max. load 400 kN) with mechanical wedge grips. Fig. 2 illustrates the setup for the bearing test. The load was applied to the specimen through a pin installed in the clevis using a torque of 6 Nm. A steel washer (inner diameter 6.3 mm, outer diameter 12 mm) was used to transmit the transverse compressive force around the periphery of the hole. Strain measurements were recorded using a 4M Digital Image Correlation (DIC) system by GOM GmbH. A dot pattern was applied to the surface of both the specimen and the bearing fixture to facilitate strain tracking, allowing the determination of local displacements δ_1 and δ_2. Using these local displacements, the bearing strain can be calculated according to the following formula (3), where D denotes the diameter of the hole and K is a factor equal to 1.0 for double shear tests:

$$\sigma_i^{br} = \frac{(\delta_1 + \delta_2)/2}{K \cdot D} \tag{3}$$

The bearing stress was determined using the following Eq. (4), in which h denotes the thickness of the specimen, k is the load per hole factor with a value of 1.0 for the tests carried out in this study, and P represents the applied load measured in newton.

$$\varepsilon_i^{br} = \frac{P}{k \cdot D \cdot h} \tag{4}$$

The ultimate bearing strength σ^{bru} was calculated from the maximum load P^{max}. To assess sensitivity to load bearing stress, a bearing-to-tensile ratio (BTR) was calculated using Eq. (5), while σ^{unt} denotes the tensile strength obtained from the unnotched tension tests.

$$BTR = \frac{\sigma^{bru}}{\sigma^{unt}} \tag{5}$$

In order to investigate the damage mechanisms, fracture surfaces were examined using the VHX-6000 digital microscope from Keyence Deutschland GmbH. The specimens were first embedded in the KEM15 Plus embedding resin system provided by ATM Qness GmbH. They were then gradually ground and polished on the automated Saphir 550 grinding and polishing machine, also from ATM Qness GmbH, starting with a 320-grit abrasive paper and progressing stepwise to a final polish with a 1 µm diamond suspension.

Table 3
Experimental mechanical properties of UNT and Bearing.

Layup	E^{unt} in GPa	σ^{unt} in MPa	ϵ^{unt} in %	σ^{bru} in MPa
30_LI	69.07	1224.54	1.65	1020.44
60_LI	69.94	1299.98	1.74	1202.21
30_BI_1	55.04	427.39	0.79	867.16
60_BI_1	52.15	413.83	0.80	857.16
60_BI_2	69.03	519.61	0.77	595.68

3. Results

3.1. Unnotched tension

Table 3 contains the test data of the UNT experiment. The results demonstrate that the Bio-Inspired (BI) structures exhibit significantly lower strength and fracture strain compared to the LI structures. This effect is consistent with the significantly lower content of 0° plies in the loading direction. An equal stiffness can be observed between the LI structures and the 60_BI_2 structure, which was optimized to E_{11}. In general, the LI structures exhibited spontaneous brittle failure due to fibre breakage, whereas the BI showed a gradual fibre matrix failure along a helical crack path beginning in the plies oriented at $\pm\ \alpha$. This type of failure in Bouligand structures has been reported in several publications [9,10]. On the basis of the test data, no significant influence of the ply thickness can be determined.

3.2. Load-bearing

In the following section, the results of bearing experiments will be displayed and discussed. Fig. 4 illustrates the experimental data of the bearing tests and Table 3 showing the ultimate bearing strength as a function of the bearing strain. From Fig. 4 it is evident that the LI structures exhibit the highest bearing strengths. Furthermore, a significant enhancement of 17.80 % in ultimate bearing strength is observed when comparing the 30_LI specimens with the 60_LI specimens, with the latter exhibiting a bearing strength of 1202.21 MPa. This improvement is attributed to the increased layer thickness of the laminate, as both configurations share an identical layup. Moreover, it is evident that the BI specimens generally exhibit lower bearing strengths. In particular, the 60_BI_2 specimen demonstrates the lowest ultimate bearing strength, measuring approximately 595.68 MPa. The 30_BI_1 and 60_BI_1 samples demonstrate approximately 44.80 % higher strengths compared to the 60_BI_2 structure. However, these values are still 28.30 % lower than those of the 60_LI and 15.50 % lower than the 30_LI specimens.

Comparing the tensile strength of the unnotched tension specimens with the ultimate bearing strength shown in Fig. 5 reveals an intriguing correlation. The BI, particularly those with larger stacking angles, exhibit significantly higher ultimate bearing strength relative to their tensile strength. Specifically, the 30_BI_1 and 60_BI_1 configurations demonstrate an increase in ultimate bearing strength of 101 %and 110 %, respectively, compared to their tensile strength (see Fig. 5). In contrast, the LI structures show a decrease in stress under bearing conditions. This enhancement can be attributed to the fact that BI with larger stacking angles better accommodates the stress distribution generated around the bolt, as the fibre arrangement more closely follows the stress pattern shown in Fig. 2 right.

Fig. 6 shows the representative fracture patterns of the various laminate structures, with the note that the thickness of the layer does not influence the failure mode. The fracture pattern of the LI structures shows a mixed mode failure (Fig. 6 a-b) between shear out and bearing failure concentrated around the bolt in loading direction and therefore behaves contrary to expectations. In Fig. 6 (b-c), it can be observed that fibre kinking occurred during testing, manifesting as an S-shaped curve through the laminate and leading to delamination in the region

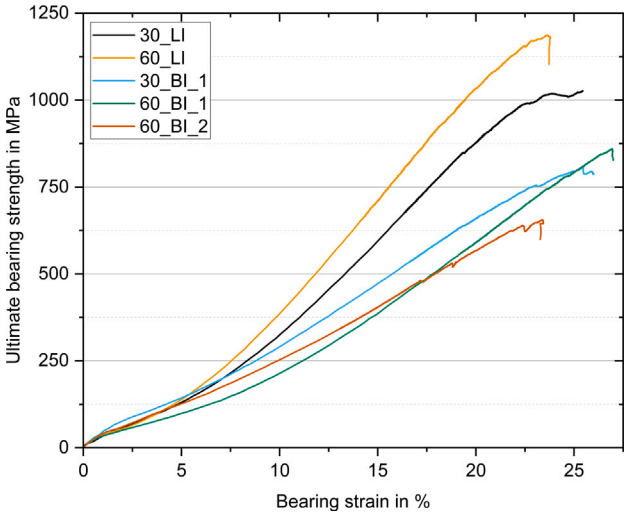

Fig. 4. Stress–strain-diagram of bearing experiments.

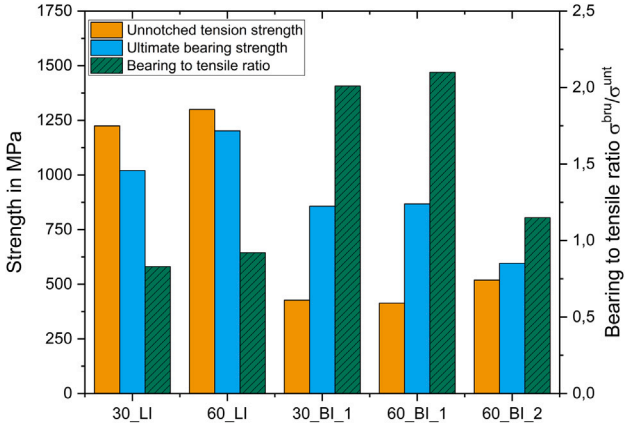

Fig. 5. Comparison of tensile strength, ultimate bearing strength and bearing to tensile ratio.

of the 0° fibres. In the BI, the fracture patterns vary significantly. In both configurations, 30_BI_1 and 60_BI_1, a combination of the intended bearing failure and a failure mode that is not classified according to the standard, characterized by helical cracks, occurs. Continuous failure through helical cracks in Bouligand structures has been described in the literature [8–10] before, but never in connection with bearing failures. For the 60_BI_2 configuration, failure was predominantly governed by helicoidal cracking, with cracks propagating towards the top of the specimen. Based on these observations, it can be hypothesized that with decreasing stack angle in combination with smaller pitch angle, the helical crack growths further towards the edges of the specimens. In Fig. 6 e, f, h, and i, helical cracks are clearly visible. These helical cracks also propagate in an S-shaped pattern, with the inflection point located in the region of the 0° fibre orientation. Unlike the delaminations observed in the LI specimens, the BI specimens predominantly exhibit helical cracks, with delamination being largely suppressed.

4. Conclusion

This study highlights the significant potential for translating biological structural principles, which have been continuously optimized through evolution to withstand specific load conditions, into technical engineering applications. The comparison between the loading introduction and Bouligand layups provided valuable insight into their mechanical performance characteristics. Although the unnotched tension

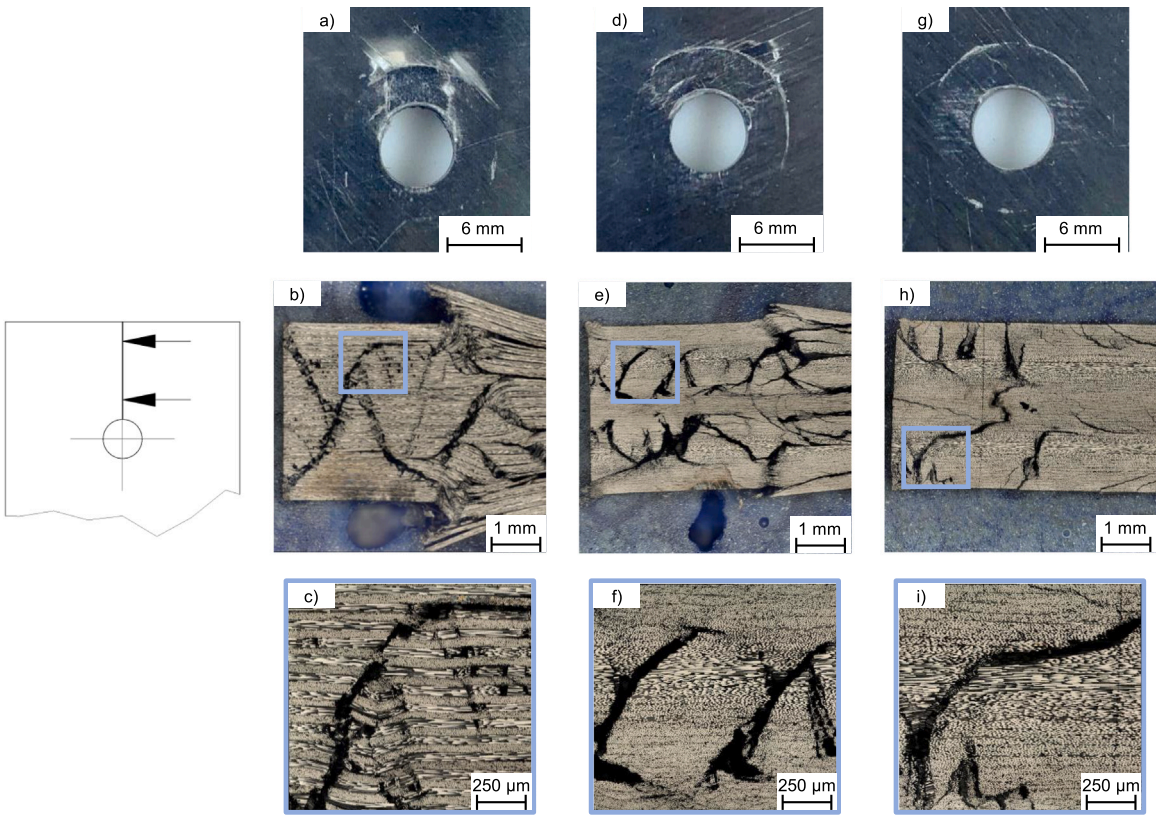

Fig. 6. Representative micrographs of composite specimens after bearing tests; (a-c) 60_LI, (d-f) 60_BI_1, (g-i) 60_BI_2.

Bouligand specimens exhibited lower tensile strength relative to load introduction layups, the 60_BI_2 partial Bouligand layup reached comparable stiffness values. Furthermore, the maximum bearing strength of the Bouligand structures, particularly those with larger stacking angles, exceeded that of the UNT samples by 100 %. This remarkable improvement in bearing capacity is indicative of the superior load distribution capabilities inherent to the Bouligand architecture, which more effectively mitigates stress concentrations around the fastener holes. Due to the radially homogeneous fibre orientation, it can be assumed that rotationally movable components, such as aircraft air brakes subjected to off-axis loading, are capable of accommodating varying load directions during operation due to the presence of a hinge, independent of their initial orientation. In contrast, off-axis loading is expected to have a more pronounced impact on the strength of LI structures. In general, these findings demonstrate that bio-inspired laminate configurations, derived from biologically occurring fibre arrangements, offer promising avenues for the development of advanced composite materials with tailored mechanical properties for engineering applications where bearing strength and damage tolerance are critical.

CRediT authorship contribution statement

Marcel Neubacher: Writing – original draft, Visualization, Methodology, Investigation, Formal analysis, Conceptualization. **Farida Touni:** Writing – original draft, Visualization, Methodology, Investigation, Formal analysis, Conceptualization. **Kohei Yamada:** Writing – review & editing, Methodology, Investigation. **Masaaki Nishikawa:** Writing – review & editing, Supervision, Project administration, Funding acquisition. **Bodo Fiedler:** Writing – review & editing, Supervision, Project administration, Methodology, Investigation, Funding acquisition, Conceptualization.

Declaration of competing interest

The authors declare that they have no known competing financial interests or personal relationships that could have appeared to influence the work reported in this paper.

Acknowledgements

The authors gratefully acknowledge the support of the DAAD (Project: 57710630) and the German Research Foundation (DFG, project number 513556749) for funding this project.

Data availability

Data will be made available on request.

References

[1] S. Sihn, R. Kim, K. Kawabe, S. Tsai, Experimental studies of thin-ply laminated composites, Compos. Sci. Technol. 67 (6) (2007) 996–1008, http://dx.doi.org/10.1016/j.compscitech.2006.06.008, URL https://linkinghub.elsevier.com/retrieve/pii/S0266353806002168.

[2] K. Kawabe, S. Tomoda, T. Matsuo, Pneumatic process for spreading reinforcing fiber tow, in: International SAMPE Symposium and Exhibition (Proceedings), vol. 42, 1997, pp. 65–76, Issue: 1 Type: Conference paper. URL https://www.scopus.com/inward/record.uri?eid=2-s2.0-00307195898&partnerID=40&md5=1a2998a96b72aae5587902e3b1b66023.

[3] A. Arteiro, C. Furtado, G. Catalanotti, P. Linde, P. Camanho, Thin-ply polymer composite materials: A review, Compos. Part A: Appl. Sci. Manuf. 132 (2020) 105777, http://dx.doi.org/10.1016/j.compositesa.2020.105777, URL https://linkinghub.elsevier.com/retrieve/pii/S1359835X20300154.

[4] A. Arteiro, G. Catalanotti, J. Xavier, P. Camanho, Notched response of non-crimp fabric thin-ply laminates, Compos. Sci. Technol. 79 (2013) 97–114, http://dx.doi.org/10.1016/j.compscitech.2013.02.001, Publisher: Elsevier BV. URL https://linkinghub.elsevier.com/retrieve/pii/S0266353813000390.

[5] R. Amacher, J. Cugnoni, J. Botsis, L. Sorensen, W. Smith, C. Dransfeld, Thin ply composites: Experimental characterization and modeling of size-effects, Compos. Sci. Technol. 101 (2014) 121–132, http://dx.doi.org/10.1016/j.compscitech.2014.06.027, URL https://linkinghub.elsevier.com/retrieve/pii/S0266353814002280.

[6] J. Cugnoni, R. Amacher, S. Kohler, J. Brunner, E. Kramer, C. Dransfeld, W. Smith, K. Scobbie, L. Sorensen, J. Botsis, Towards aerospace grade thin-ply composites: Effect of ply thickness, fibre, matrix and interlayer toughening on strength and damage tolerance, Compos. Sci. Technol. 168 (2018) 467–477, http://dx.doi.org/10.1016/j.compscitech.2018.08.037, URL https://linkinghub.elsevier.com/retrieve/pii/S0266353818302756.

[7] L. Mencattelli, S.T. Pinho, Ultra-thin-ply CFRP Bouligand bio-inspired structures with enhanced load-bearing capacity, delayed catastrophic failure and high energy dissipation capability, Compos. Part A: Appl. Sci. Manuf. 129 (2020) 105655, http://dx.doi.org/10.1016/j.compositesa.2019.105655, URL https://linkinghub.elsevier.com/retrieve/pii/S1359835X1930404X.

[8] J. Körbelin, P. Goralski, B. Kötter, F. Bittner, H.-J. Endres, B. Fiedler, Damage tolerance and notch sensitivity of bio-inspired thin-ply Bouligand structures, Compos. Part C: Open Access 5 (2021) 100146, http://dx.doi.org/10.1016/j.jcomc.2021.100146, URL https://linkinghub.elsevier.com/retrieve/pii/S2666682021000414.

[9] H. Wang, C. Wang, P.J. Hazell, A. Wright, Z. Zhang, X. Lan, K. Zhang, M. Zhou, Insights into the high-velocity impact behaviour of bio-inspired composite laminates with helicoidal lay-ups, Polym. Test. 103 (2021) 107348, http://dx.doi.org/10.1016/j.polymertesting.2021.107348, URL https://linkinghub.elsevier.com/retrieve/pii/S0142941821002932.

[10] A. Sharma, N.K. Shukla, M.-O. Belarbi, M. Abbas, A. Garg, L. Li, J. Bhutto, A. Bhatia, Bio-inspired nacre and helicoidal composites: From structure to mechanical applications, Thin-Walled Struct. 192 (2023) 111146, http://dx.doi.org/10.1016/j.tws.2023.111146, URL https://linkinghub.elsevier.com/retrieve/pii/S0263823123006249.

[11] H. Luo, H. Wang, Z. Zhao, H. Xue, Y. Li, Experimental and numerical investigation on the failure behavior of Bouligand laminates under off-axis open-hole tensile loading, Compos. Struct. 313 (2023) 116932, http://dx.doi.org/10.1016/j.compstruct.2023.116932, URL https://linkinghub.elsevier.com/retrieve/pii/S0263822323002763.

[12] M. Shan, R. Zhang, F. Liu, L. Zhao, A characteristic curve including hygrothermal effects for predicting the failure of composite multi-bolt joints, Compos. Commun. 36 (2022) 101384, http://dx.doi.org/10.1016/j.coco.2022.101384, URL https://linkinghub.elsevier.com/retrieve/pii/S2452213922003266.

[13] S. Sathiya Naarayan, D. Pavan Kumar, S. Chandra, Implication of unequal rivet load distribution in the failures and damage tolerant design of metal and composite civil aircraft riveted lap joints, Eng. Fail. Anal. 16 (7) (2009) 2255–2273, http://dx.doi.org/10.1016/j.engfailanal.2009.03.016, URL https://linkinghub.elsevier.com/retrieve/pii/S135063070900048X.

[14] G. Catalanotti, P.P. Camanho, A semi-analytical method to predict net-tension failure of mechanically fastened joints in composite laminates, Compos. Sci. Technol. 76 (2013) 69–76, http://dx.doi.org/10.1016/j.compscitech.2012.12.009, URL https://www.sciencedirect.com/science/article/pii/S0266353812004162.

[15] P.P. Camanho, C.M.L. Tavares, R.d. Oliveira, A.T. Marques, A.J.M. Ferreira, Increasing the efficiency of composite single-shear lap joints using bonded inserts, Compos. Part B: Eng. 36 (5) (2005) 372–383, http://dx.doi.org/10.1016/j.compositesb.2005.01.007, URL https://www.sciencedirect.com/science/article/pii/S1359836805000235.

[16] P.P. Camanho, F.L. Matthews, Stress analysis and strength prediction of mechanically fastened joints in FRP: a review, Compos. Part A: Appl. Sci. Manuf. 28 (6) (1997) 529–547, http://dx.doi.org/10.1016/S1359-835X(97)00004-3, URL https://www.sciencedirect.com/science/article/pii/S1359835X97000043.

[17] C.J. Cameron, J. Larsson, M.S. Loukil, T. Murtagh, P. Wennhage, Bearing strength performance of mixed thin/thick-ply, quasi-isotropic composite laminates, Compos. Struct. 261 (2021) 113312, http://dx.doi.org/10.1016/j.compstruct.2020.113312, Publisher: Elsevier BV. URL https://linkinghub.elsevier.com/retrieve/pii/S0263822320332384.

[18] B. Kötter, K. Yamada, J. Körbelin, K. Kawabe, M. Nishikawa, M. Hojo, B. Fiedler, Steel foil reinforcement for high performance bearing strength in Thin-Ply composites, Compos. Part C: Open Access 4 (2021) 100085, http://dx.doi.org/10.1016/j.jcomc.2020.100085, Publisher: Elsevier BV. URL https://linkinghub.elsevier.com/retrieve/pii/S2666682020300852.

[19] H. Quan, W. Yang, E. Schaible, R.O. Ritchie, M.A. Meyers, Novel defense mechanisms in the armor of the scales of the “Living Fossil” coelacanth fish, Adv. Funct. Mater. 28 (46) (2018) 1804237, http://dx.doi.org/10.1002/adfm.201804237, URL https://onlinelibrary.wiley.com/doi/10.1002/adfm.201804237.

[20] Y. Zhang, G. Tan, M. Zhang, Q. Yu, Z. Liu, Y. Liu, J. Zhang, D. Jiao, F. Wang, L. Zhuo, Z. Zhang, R.O. Ritchie, Bioinspired tungsten-copper composites with Bouligand-type architectures mimicking fish scales, J. Mater. Sci. Technol. 96 (2022) 21–30, http://dx.doi.org/10.1016/j.jmst.2021.04.022, URL https://linkinghub.elsevier.com/retrieve/pii/S1005030221004503.

[21] S. Yin, R. Yang, Y. Huang, W. Guo, D. Chen, W. Zhang, M. Ren, Y. Zhou, J. Xu, Toughening mechanism of coelacanth-fish-inspired double-helicoidal composites, Compos. Sci. Technol. 205 (2021) 108650, http://dx.doi.org/10.1016/j.compscitech.2021.108650, URL https://linkinghub.elsevier.com/retrieve/pii/S0266353821000063.

[22] ASTM D 3039/D 3039M - 00 Standard Test Method for Tensile Properties of Polymer Matrix Composite Materials, West Conshohocken, PA, 2000.

[23] ASTM D5961/D 5961M-01 Standard Test Method for Bearing Response of Polymer Matrix Composite Laminates, 2017.